

# Fast-response switchable lens for 3D and wearable displays

Yun-Han Lee, Fenglin Peng, and Shin-Tson Wu\*

CREOL, The College of Optics and Photonics, University of Central Florida, Orlando, Florida 32816, USA  
\*swu@ucf.edu

**Abstract:** We report a switchable lens in which a twisted nematic (TN) liquid crystal cell is utilized to control the input polarization. Different polarization state leads to different path length in the proposed optical system, which in turn results in different focal length. This type of switchable lens has advantages in fast response time, low operation voltage, and inherently lower chromatic aberration. Using a pixelated TN panel, we can create depth information to the selected pixels and thus add depth information to a 2D image. By cascading three such device structures together, we can generate 8 different focuses for 3D displays, wearable virtual/augmented reality, and other head mounted display devices.

©2016 Optical Society of America

OCIS codes: (230.3720) Liquid-crystal devices; (080.3620) Lens system design.

---

## References and links

1. O. Cakmakci and J. Rolland, "Head-worn displays: a review," *J. Display Technol.* **2**(3), 199–216 (2006).
2. B. Furht, *Handbook of Augmented Reality* (Springer, 2011).
3. H. Ren and S. T. Wu, *Introduction to Adaptive Lenses* (Wiley, 2012).
4. K. Akeley, S. J. Watt, A. R. Girshick, and M. S. Banks, "A stereo display prototype with multiple focal distances," *ACM Trans. Graph.* **23**(3), 804–813 (2004).
5. S. Liu and H. Hua, "A systematic method for designing depth-fused multi-focal plane three-dimensional displays," *Opt. Express* **18**(11), 11562–11573 (2010).
6. S. Ravikumar, K. Akeley, and M. S. Banks, "Creating effective focus cues in multi-plane 3D displays," *Opt. Express* **19**(21), 20940–20952 (2011).
7. B. T. Schowengerdt and E. J. Seibel, "True 3-D scanned voxel displays using single or multiple light sources," *J. Soc. Inf. Disp.* **14**(2), 135 (2006).
8. S. W. Lee and S. S. Lee, "Focal tunable liquid lens integrated with an electromagnetic actuator," *Appl. Phys. Lett.* **90**(12), 121129 (2007).
9. U. Efron, *Spatial Light Modulator Technology: Materials, Devices, and Applications* (Marcel Dekker, 1994).
10. E. J. Fernández, B. Považay, B. Hermann, A. Unterhuber, H. Sattmann, P. M. Prieto, R. Leitgeb, P. Ahnelt, P. Artal, and W. Drexler, "Three-dimensional adaptive Optics ultrahigh-resolution optical coherence tomography using a liquid crystal spatial light modulator," *Vision Res.* **45**(28), 3432–3444 (2005).
11. M. B. North-Morris, J. VanDelden, and J. C. Wyant, "Phase-shifting birefringent scatterplate interferometer," *Appl. Opt.* **41**(4), 668–677 (2002).
12. H. O. Saldner and J. M. Huntley, "Profilometry using temporal phase unwrapping and a spatial light modulator-based fringe projector," *Opt. Eng.* **36**(2), 610–615 (1997).
13. M. Schadt and W. Helfrich, "Voltage-dependent optical activity of a twisted nematic liquid crystal," *Appl. Phys. Lett.* **18**(4), 127 (1971).
14. H. Ren, S. Xu, Y. Liu, and S. T. Wu, "Switchable focus using a polymeric lenticular microlens array and a polarization rotator," *Opt. Express* **21**(7), 7916–7925 (2013).
15. R. Zhu, S. Xu, Q. Hong, S. T. Wu, C. Lee, C. M. Yang, C. C. Lo, and A. Lien, "Polymeric-lens-embedded 2D/3D switchable display with dramatically reduced crosstalk," *Appl. Opt.* **53**(7), 1388–1395 (2014).
16. A. Chao, K. T. Huang, C. W. Tsai, Y. W. Hung, H. F. Cheng, W. Yeh, C. H. Yu, and H. H. Wu, "The fastest response TN-Type TFT LCD of the world likes OCB level," *SID Int. Symp. Digest Tech. Papers* **38**(1), 603–606 (2007).
17. S. Gauza, X. Zhu, W. Piecek, R. Dabrowski, and S. T. Wu, "Fast switching liquid crystals for color-sequential LCDs," *J. Display Technol.* **3**(3), 250–252 (2007).
18. Y. Huang, C.-H. Wen, and S.-T. Wu, "Polarization-independent and submillisecond response phase modulators using a 90° twisted dual-frequency liquid crystal," *Appl. Phys. Lett.* **89**(2), 021103 (2006).
19. C. H. Gooch and H. A. Tarry, "The optical properties of twisted nematic liquid crystal structures with twisted angles  $\leq 90^\circ$ ," *J. Phys. D.* **8**(13), 1575–1584 (1975).

## 1. Introduction

Virtual reality and augmented reality [1, 2] are emerging wearable display technologies for immersive video games and interactive 3D graphics. A critical issue of these display devices is distance matching. For 3D displays based on sending different images to different eyes, e.g. Oculus Rift™, the perceived image may locate at a distance different from the eye's focal length, thus causing eye-brain conflict and strain. For devices such as Google Glass™, since only one eye is receiving information, the above mentioned problem is mitigated. Instead, its major problem is the mismatch between the distance of displayed image and the surrounding image because the displayed image remains at a certain plane. In this case, the viewer cannot focus at the image from the device and the surrounding objects simultaneously. In either case mentioned above, the need for a tunable/switchable lens is apparent. Even though several types of tunable/switchable lenses have been proposed before [3], according to [4–6] to achieve a depth-fused 3D display, which forms the sense of 3D through fast switching between different focuses, it is required to switch between at least six image planes while keeping the same angular size. For a display with 60 frames per second, when switching between six focal lengths in a field sequential manner, the response time should be less than 3 ms. Among many proposed tunable/switchable lenses/ mirrors, only few candidates can achieve such a fast response time. Microelectromechanical systems (MEMS), in particular, a deformable membrane mirror device [7] is a promising candidate, while current-induced shape-changing lens [8] is another option. However, the former is relatively difficult to fabricate for large aperture and it is a reflective device, while the latter is essentially a current device, which consumes more power.

In addition to flat panel displays, liquid crystals (LCs) have also been widely used in adaptive optics [9], optical coherence tomography [10], interferometry [11] and surface profilometry [12]. In this paper, we demonstrate an LC focus-switching device for 3D head-mounted displays. The LC device used here is a 90° twisted nematic (TN) cell [13]. TN is an electrically tunable achromatic half-wave ( $\lambda/2$ ) plate and has been used as a polarization switch for adaptive lens [14, 15]. For a linearly polarized input light, say p-wave, the output light can be converted to s-wave if the applied voltage is off ( $V = 0$ ) or it remains p-wave if  $V \gg V_{th}$  (threshold voltage). For a commercial TN display, the response time can be as fast as 2 ms [16] or sub-millisecond if the cell gap is reduced to 1.6  $\mu\text{m}$  [17] or a dual-frequency LC [18] is employed, while keeping the driving voltage below 10  $V_{rms}$ . Also, due to its achromatic nature, TN-assisted lens system has very little chromatic aberration. With these advantages, here we incorporate a TN cell as a polarization switch in our optical system. The outgoing beam would travel at different paths, depending on the p- or s-wave, when entering a polarization dependent component such as a polarizing beam splitter (PBS), a wire-grid polarizer (WGP), a dual brightness enhancement film (DBEF), or a uniaxial/biaxial plate. Upon properly controlling and recombining the output waves with retardation films, lenses, and mirrors, this path difference can be exploited to change the effective focal distance or image planes and thus effectively forms a fast switchable lens. Following this principle, different setups, such as the number of lenses/mirrors, focal length of each lens/mirror, the distance between the lens/mirror, the switching power and the direction of outgoing light, can be utilized for different applications. A special advantage of this device is that it can create depth information to a 2D image when the TN panel is pixelated.

## 2. Experimental

Figure 1 shows the experimental setup to realize the focus switching. A 90° TN cell was used to switch the polarization of the input beam between s-wave and p-wave. To obtain fast response time, we infiltrated a low viscosity LC mixture DIC-LC2 ( $\gamma = 32 \text{ mPa} \cdot \text{s}$ ,  $\Delta n = 0.121$  and  $\Delta \epsilon = 2.0$ ) into a 4.9- $\mu\text{m}$  TN cell. By applying 10  $V_{rms}$  of an AC voltage (1 kHz

frequency) to the TN cell, which was sandwiched between crossed polarizers, we measured the rise time and the decay time to be 4.3 ms and 1.0 ms, respectively. Note that here the response time was not optimized due to the limited TN cells we have. In principle, to meet Gooch—Tarry condition [19] for achromatic polarization rotation, the optimal TN cell gap should satisfy  $d\Delta n/\lambda = \sqrt{3}/2$ , where  $d$  is the cell gap and the wavelength  $\lambda$  is usually chosen to be 550 nm. Therefore, for DIC-LC2 ( $\Delta n = 0.121$ ), the optimized cell gap is  $3.9 \mu\text{m}$ . Since the response time is proportional to  $d^2$ , by reducing the cell gap from  $4.9 \mu\text{m}$  to  $3.9 \mu\text{m}$ , the rise time and the decay time can reach 2.8 ms and 0.6 ms, respectively. By using a higher birefringence LC material with a thinner cell gap, we can even obtain sub-millisecond response time [17]. As Fig. 1 depicts, our optical system consisted of a broadband PBS, two broadband  $\lambda/4$  polymeric retarder films (450–700 nm, Edmund Optics), two lenses (L1 and L2), and two flat mirrors (M1 and M2). The first lens L1 ( $f_1 = 10 \text{ cm}$ ) was located at  $P = 15 \text{ cm}$  away from the object. After passing through L1, one polarization (red arrow, say s-wave) passed straight through PBS,  $45^\circ$ -oriented (with respect to the polarization, in the plane that was perpendicular to the propagation direction)  $\lambda/4$  plate, and reached M1. Upon reflection, the beam passed through the  $\lambda/4$  plate one more time and its polarization state was converted to p-wave. Thus, it was reflected by the PBS toward L2 ( $f_2 = 20 \text{ cm}$ ). The total path length from L1 to L2 for the red route is  $d_1 = 43 \text{ cm}$ . On the other hand, the other polarization (blue arrow, say p-wave) was reflected first by the PBS toward the  $45^\circ$ -oriented  $\lambda/4$  plate and M2. Upon reflection from M2, the beam passing through the  $\lambda/4$  plate one more time and was converted to s-wave. As a result, it passed through the PBS and L2. Since M2 was placed farther away from PBS than M1, its path was longer. The total path length from L1 to L2 for the blue route is  $d_2 = 48 \text{ cm}$ , which is longer than  $d_1$ . A digital CCD camera was located at  $D = 23 \text{ cm}$  away from L2.

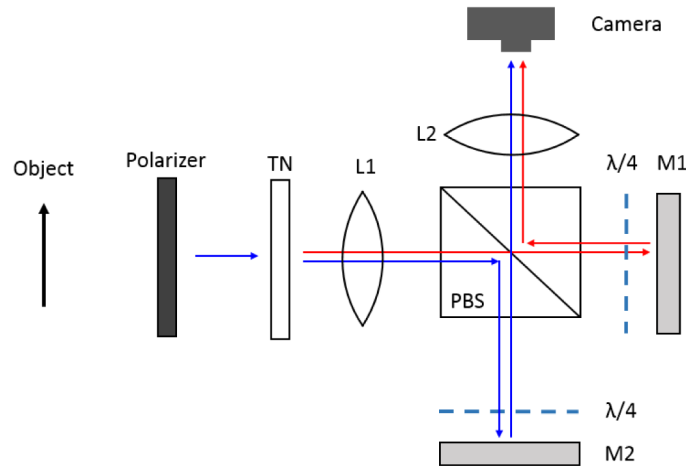


Fig. 1. The experimental setup to realize path length difference for two different polarizations. The two paths for s- and p- polarizations are denoted as red and blue arrows. The path difference is introduced by placing mirrors M1 and M2 at different distances from PBS.

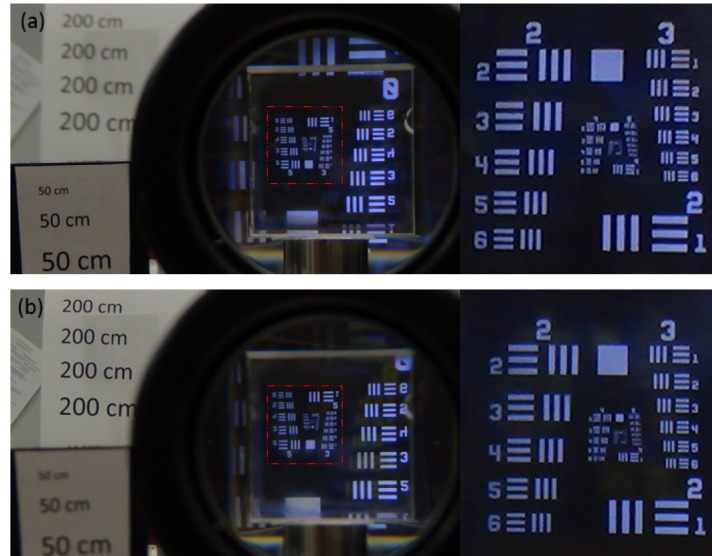


Fig. 2. When looking into the PBS, the switching between two paths results in different images. Photo (a) shows the image corresponding to the red line in Fig. 2; the image was located at 50 cm away from the camera. Photo (b) shows the image corresponding to the blue line in Fig. 2; the image was located at 200 cm away. The other images beside the main images are results of surface reflection from other components. Photos on the right side are the enlarged and inverted pictures of the red dashed blocks.

### 3. Results and discussion

The resultant images are shown in Fig. 2. As one looks through the PBS, two different inverted images can be observed upon switching-on and -off the TN cell. We can clearly see the change in image planes from the references, which are located at 50 cm and 200 cm away from the camera, respectively. The angular size in the longer path (blue line in Fig. 1) is slightly larger than the size in the shorter path (red line in Fig. 1). Note that some other blurred images are present along with the main images, resulting from surface reflections. These ghost images can be easily eliminated by lamination and integration, or anti-reflection coating of the components. Slight aberration can be seen and was mainly from the small acceptance angle of PBS. The observed bluish color results from the employed bluish LED flashlight. To reduce aberration, WGP, DBEF or uniaxial/biaxial plates can be considered.

Next, we study the image-to-eye distance and the angular size between these two paths analytically. Assuming paraxial and thin lens condition, from the conjugation equation [20]:

$$1/L' - 1/L = 1/f, \quad (1)$$

where  $L'$  and  $L$  denote the location of the image and the object, respectively, while  $f$  denotes the focal length of the thin lens. Notice that  $L$  is negative for it is located before the lens. For lens with non-negligible thickness more detailed calculation should be performed. We apply the conjugation equation once for each lens. After some algebra, we derive the image-to-eye/camera distance as:

$$L_e = D - \frac{(d + \frac{f_1 P}{f_1 - P})f_2}{d + \frac{f_1 P}{f_1 - P} - f_2}, \quad (2)$$

where  $D$  stands for the distance from the final lens to eye/camera, and  $d$  denotes the distance between two lenses:  $d_1$  and  $d_2$  for the shorter and longer paths, respectively. The image magnification is expressed as [20]:

$$M = L'/L. \quad (3)$$

Accordingly, we calculate the magnification in our system:

$$M = \frac{f_1}{f_1 - P} \frac{f_2}{f_2 - f_1 P / (f_1 - P) - d}. \quad (4)$$

Finally, we can estimate the angular size:

$$A = \arctan\left(\frac{S_0 M}{L_e}\right), \quad (5)$$

where  $S_0$  is the original object size.

These equations indicate that, by switching the TN cell on and off, we can equivalently change the lens distance ( $d$ ) between  $d_1$  and  $d_2$ . The image angular size ( $A$  in Eq. (5)) as well as the image-to-eye distance ( $L_e$  in Eq. (2)) are switched correspondingly. Using the previous experimental parameters, we adjust  $D$  while fixing other parameters to see the corresponding change in the angular sizes for the two paths. Assuming the object size was 5 cm, we plotted the result in Fig. 3. The angular size for the image in shorter path increases faster than the one for the longer path, and at  $D = 20$  cm, which is the focal length ( $f_2$ ) of L2, these two lines intersect. This implies that if we set the eye/camera at  $f_2$ , i.e.,  $D = f_2$ , we can obtain images with the same angular size to achieve depth-fused 3D display.

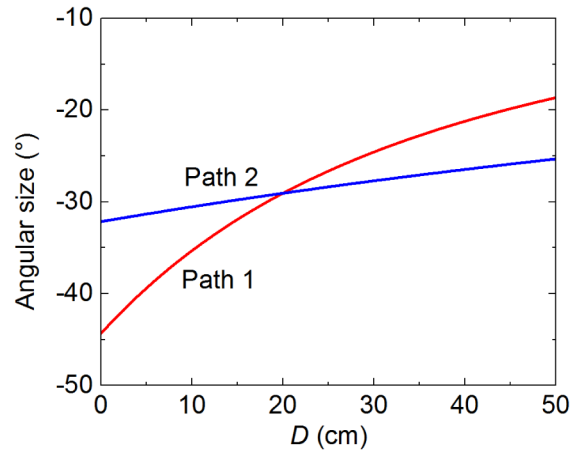


Fig. 3. Upon increasing  $D$  (the distance from L2 to camera), the angular size of the image from both paths increases but Path 1 (shorter path) increases faster. At 20 cm, these two lines coincide, resulting in the angular size of around  $-30^\circ$  (the object size is assumed to be 5 cm).

Therefore, we simplify Eqs. (2) and (5) by demanding  $D = f_2$ , and the results are reduced to:

$$L_e = \frac{f_2^2}{f_2 - \frac{f_1 P}{f_1 - P} - d}, \quad (6)$$

$$A = \arctan\left(\frac{S_0 f_1}{f_1 f_2 - P}\right). \quad (7)$$

We see that Eq. (6) is still dependent on  $d$  while Eq. (7) is no longer dependent on  $d$ . This means when switching the image-to-eye distance by turning on/off the TN cell, although the effective distance between the lenses changes, the angular sizes remain unchanged.

Next, we would like to discuss an even more simplified case. In this case, we remove L1 such that only one lens remains in the system. Even though flexibility is compromised, this configuration is particularly useful due to its simplicity. The mirrors can also be replaced with wire-grid polarizers or DBEFs for see-through applications. The corresponding formula for image-to-eye distance and angular size can be obtained by setting  $f_1$  to infinity and  $d$  to zero in Eq. (6) and Eq. (7), and we obtain:

$$L_e = \frac{f^2}{f - P}, \quad (8)$$

$$A = \arctan\left(\frac{S_0}{f}\right), \quad (9)$$

where  $f$  denotes the focal length. Note that since there is only one lens in this case,  $d$  no longer exists, and the switching of TN essentially switches between two object distances; we denote them as  $P_1$  and  $P_2$ , with  $P_2 > P_1$  and  $\Delta d = P_2 - P_1$ . From Eq. (8), we can see that, for example, to switch from infinity to 30 cm, we need  $P_2 \approx f$ , while  $P_1 = f - f^2 / 30$ , and thus we need  $\Delta d = f^2 / 30$ , with units in cm. This implies that when the focal length is larger, longer path difference is needed.



Fig. 4. When looking into the PBS, the switching between two paths results in different images as shown above. The left photo shows the image when the light travels through the shorter path, with the image being 40 cm away from the camera, while the right photo shows the image when the light travel the longer path, with the image being 200 cm away. Only one lens with  $f$  being 25 cm was used.

To experimentally demonstrate this further simplified device, we remove the lens L1 from Fig. 1. Mirrors were positioned such that  $P_1 = 11$  cm,  $P_2 = 22$  cm, the focal length was 25 cm, and the camera was located 25 cm away from the lens. The corresponding experimental result is shown in Fig. 4. A clear difference can be observed from the references in the photos, yet the angular sizes match very well. The reference screens were located at 40 cm and 200 cm. Again, slight aberration can be found, which mainly results from the small acceptance angle of PBS.

In above discussions we have shown two simplified device configurations. In Fig. 5, we plot some generalized device configurations. For examples, the mirrors M1 and M2 in Figs. 5(a)–5(c) could be concaved instead of flat. Green blocks denote the quarter-wave films. The two device structures as Figs. 5(a) and 5(b) depict, lead to different output directions, yet they

both have one polarization passing through PBS once and the other polarization passing through PBS multiple times. Also, one polarization is not reflected by the mirrors while the other is reflected twice. On the other hand, in Fig. 5(c), both polarizations are reflected by a mirror once and pass through the PBS twice. As shown in Fig. 5(d), we can also use a uniaxial material (denoted as a blue block), which is favored for compact size and lightweight, instead of a PBS to produce the needed path difference. For general embodiments, it is not necessary for the concave mirrors and convex lenses to be laminated onto the PBS or the uniaxial/biaxial material nor are they required to be concave/convex/flat; these components can be engineered with different shape and different distance for a particular purpose. To further reduce chromatic aberration, one can also add extra lenses to form apochromatic lenses. The optical path length difference in Figs. 5(a)–5(c) can be tailored easily through properly positioning the mirrors. While in Fig. 5(d), a uniaxial/biaxial plate is exploited to provide the path difference, which is decided by the different refractive indices ( $n_1$ ,  $n_2$ , and  $n_3$ ) along different optic axes and the thickness  $d_0$ . For a uniaxial plate, the path difference in the lens system is  $\Delta d = d_0/n_1 - d_0/n_2$ . Since the TN cell can be either embedded onto the system or placed outside the system, it is not shown in Fig. 5.

In either of these cases, the chromatic aberration is rather insignificant since PBS, TN and retardation plates are all achromatic. The main contribution of the chromatic aberration is from the lenses, and this can be reduced through adopting achromats instead of using single lenses. When only concave/convex mirrors exist, one can obtain minimal chromatic aberration.

To extend the device for multi-focus switching, we can stack more than one set of the device. Two of the possible embodiments are plotted in Fig. 6. In Fig. 6(a), three sets of PBSs and TNs, and two sets of mirrors and retardation films are integrated together with one lens. Each TN/PBS set serves as a distance switch which all together provides  $2^3$  possible image planes. In Fig. 6(b), by replacing the PBS with three uniaxial/biaxial plates, it forms a more compact device. Note that three layers are plotted with different thicknesses for versatility.

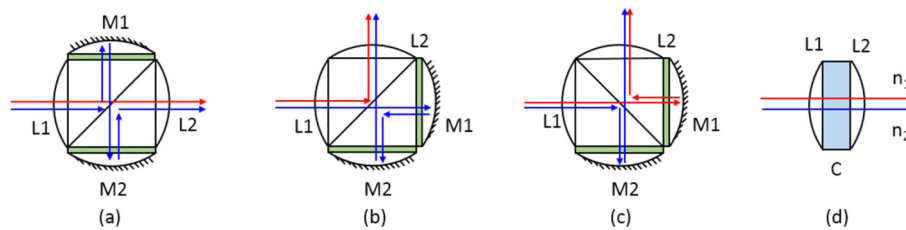


Fig. 5. Four possible device configurations with more versatility. In (a)–(c), green blocks represent the  $\lambda/4$  films. In (d), the blue block, C, denotes a uniaxial/biaxial plate.

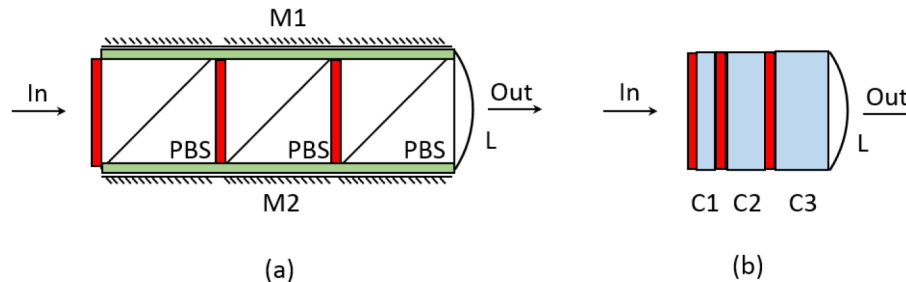


Fig. 6. Two examples of the stacked device that has  $2^3$  possible focuses. Red bars indicate the location of TN cells. Green blocks in (a) represent the  $\lambda/4$  films and the blue blocks in (b) stand for the uniaxial/biaxial plates.

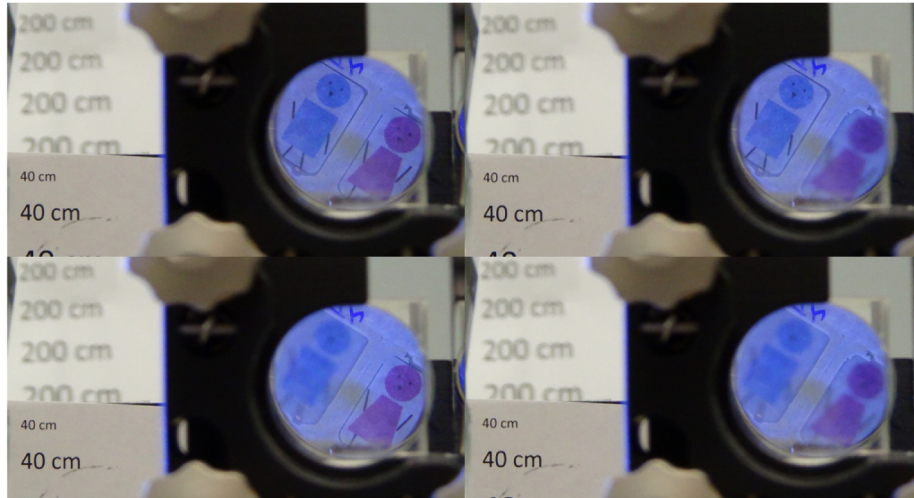


Fig. 7. An experiment using two TN cells to represent two pixels (girl and boy) to prove concept that depth information can be added to a 2D image by switching-on and -off the TN pixels.

In Fig. 7, we demonstrate that this method can provide different depth information for a 2D image. We placed two TN cells on top of a paper printed with a boy and a girl. Fixing the camera focus at 40 cm, we switched on and off separately the two TNs and we could keep both images at 40 cm, projected the girl to 200 cm away (out of the focus), projected the boy to 200 cm away, or projected both of them to 200 cm away. If we use three high resolution TN panels (without polarizers) in the stacked structure (Fig. 6(a)), then essentially we can project each pixel of an image to different desired planes and generate images with distance information.

#### 4. Conclusion

We proposed a switchable-focus lens system by using a TN cell as polarization switch to control the optical path length through the PBS and lens/mirror assembly. This focus control has the merits of fast response time, low voltage, low chromatic aberration, and simple implementation. It can create depth information for a 2D image when the TN cell is pixelated. The angular sizes of the images can be matched, and this method can be extended to form more than two switchable focal distances (or image planes) upon proper arrangement to achieve depth-fused 3D display. The proposed device has potential applications in head-mounted displays, virtual reality, augmented reality, and 3D displays.

#### Acknowledgment

The authors are indebted to AFOSR for partial financial support under contract No. FA9550-14-1-0279.